Crimson Publishers
Wings to the Research

Review Article

Multiscale Simulations of Parabolic, Elliptic and Hyperbolic, Linear PDE's Using Wavelet-based Multiresolution Analysis

ISSN: 2640-9690

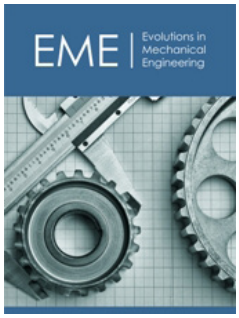

JB Allen*

Information Technology Laboratory, US Army Engineer Research and Development Center, USA

***Corresponding author:** : JB Allen, Information Technology Laboratory, US Army Engineer Research and Development Center, USA

Submission: November 15, 2024
Published: December 16, 2024

Volume 5 - Issue 5

How to cite this article: JB Allen*. Multiscale Simulations of Parabolic, Elliptic and Hyperbolic, Linear PDE's Using Wavelet-based Multiresolution Analysis. Evolutions Mech Eng. 5(5). EME.000621. 2024.
DOI: 10.31031/EME.2024.05.000621

Abstract

In this work we investigate the use of wavelet-based multiresolution analysis for scaled solutions of various linear partial differential equations. In particular, we investigate exact and scaled solutions of various parabolic, elliptic and hyperbolic partial differential equations in one and two dimensions. For the exact solutions, we utilize a standard finite difference approach with Gaussian elimination, while for the scaled solutions, we apply the wavelet-based multiresolution analysis (incorporating the Haar wavelet basis and the Schur complement). In addition to proving effective at offering scaled solutions for a select number of different partial differential equation types, we also observed that for hyperbolic equations with relatively large velocity magnitudes, an observed lag is found with respect to the wavelet-based solutions as compared to the exact solutions.

Keywords: : Wavelets; Multiresolution analysis; Scaled solutions; Partial differential equations; Schur complement

Introduction

Presently there is a growing need for multiscale characterization and analysis in a large variety of research areas. In some cases, the largest (coarse) scale features may be of greatest concern, while in other cases the smallest scale features are most critical. Still in other cases an intermediate mix over a large spectrum of scales may be of interest. While questions related to precisely what constitutes the delineation between small and large scales may never be fully settled, it is clear that many applications show a tendency toward scale interdependency, wherein a property obtained at one particular scale (be it temporal or spatial) depends on the scale immediately below or above it. In such cases, being able to decipher and appropriately resolve these interdependent scales is of paramount importance. Some of the specific research areas which have benefitted (and continue to benefit) from multiscale characterization and analysis, include; the areas of computational fluid dynamics [1-3], materials modeling and manufacturing [1,4,5], computational solid mechanics [6], weather forecast models [7,8] and others. Complementing these, there are also a growing number of joint (Multiphysics), multiscale applications, including, thermal-fluid models [9] and solid-thermal-fluid models [10], just to name a few. In addition to the aforementioned desire to better understand scale interdependency, facilitating this growth in multiscale research can be attributed to various technological advancements, including; large scale parallel computing, machine learning and artificial intelligence.

Current methods of multiscale modeling are numerous and varied. Some of the methods most predominantly used include: multigrid methods [11,12], domain decomposition methods [13,14], Fourier analysis [15], fast multipole methods [16], adaptive mesh refinement

methods [17], wavelet-based methods [18], homogenization methods [19-23] and quasi-continuum methods [24,25]. While each of these methods have provided remarkable contributions to the advancement of multiscale modeling, wavelet-based methods, particularly those leveraging the inherent advantages of Multi-Resolution Analysis (MRA) [26,27], deserve particular attention for reasons that will become apparent in subsequent sections of this work. Founded on a prescribed set of orthonormal scaling and wavelet bases functions, and leveraging the fact that these basis functions form a set of nested subspaces, wavelet-based MRA has evolved into a mature, and proven multiscale tool supporting a wide number of scientific disciplines, including applied mathematics and signal processing. Some of the past research utilizing wavelet-based MRA includes the inaugural work of Basdevant et al. [27], in which 2D turbulent flows were analyzed using both continuous and discrete wavelet transforms. Among their results, they determined that the wavelet coefficients, along with local spectra and entropy fluxes could be used to separate the various scales of the flow. Additional work includes that of Mehraeen et al. [28] who considered the use of wavelet-based MRA to analyze heterogeneous materials within a one-dimensional elastic rod. Wavelet-based MRA has also been used to solve ordinary and Partial Differential Equations (PDE's) at multiple scales [19-23,29], particularly those that can be linearized and set within the familiar linear matrix or operator framework; LU=F. In this paper we intend to augment the above-mentioned wavelet-based MRA research portfolio, and investigate the approach with respect to both 1D and 2D PDE's of various types; including, parabolic, elliptical, and hyperbolic. In addition to solving the candidate PDE's at various scales, for comparison purposes we also compute the 'exact' solution using traditional finite difference techniques.

Method

Wavelets and wavelet transforms

Like Fourier transforms, wavelet-based transforms utilize orthonormal basis functions. However, unlike Fourier transforms, these basis functions allow for the simultaneous interpretation of signals (or functions) in time and frequency. The functions themselves are made up of short duration pulses of varying frequency and wavelength and can be written in terms of both scaling ϕ and wavelet functions ψ. Written as a function of time, a continuous wavelet function may be written as:

$$\psi_{a,b}(t) = \frac{1}{\sqrt{a}}\psi\left(\frac{t-b}{a}\right) \quad (1)$$

Where a and b are the well-known scaling and translation parameters. Its corresponding transform, W can thus be written as:

$$W(a,b) = \int_{t_1}^{t_2} f(t)\ \psi_{a,b}(t)dt \quad (2)$$

Different values of a and b allow for the creation of a set of orthonormal basis functions that span a given wavelet basis function space. In addition to various continuous wavelet types (i.e., Morlet [30]), there are also various discrete forms, with the latter generally being more appropriate for computational modeling. Some of the commonly used discrete wavelet functions include the Haar [31], and Daubechies [18] waveforms. While the Haar [31] scaling and wavelet functions (shown in Figure 1(a)) is composed of relatively simple rectangular waveforms, the Daubechies [18] functions (Figure 1(b) are much more complicated. In fact, this wavelet is known to be a fractal (something that has fractional dimensions) that allow it to have detailed structure at arbitrarily small scales.

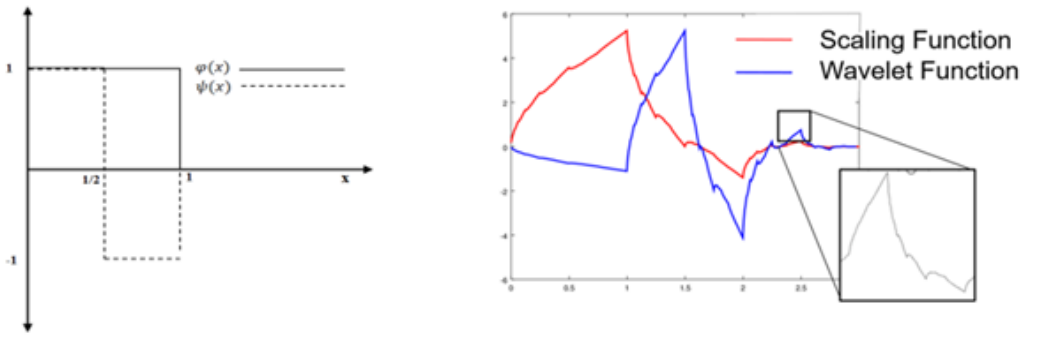

(a) Haar [31] scaling and wavelet function, $\varphi_{0,0}$, and $\psi_{0,0}$, respectively.

(b) Daubechies [18] scaling and wavelet function,

Figure 1: Representative Haar [31] & Daubechies [18] scaling and wavelet functions.

Wavelet-based multiresolution analysis

While the theory and background ascribed to 1D wavelet-based MRA has been well described in various other works [19-23], the same cannot necessarily be said for 2D and higher dimensions. In this section, we provide an overview of the process. Multidimensional, Wavelet-based MRA [32] begins with a linear matrix equation of the form typical of discretized boundary value problems, shown as:

$$LU = F \quad (3)$$

where L is a bounded linear matrix operator and U is the solution vector of unknowns. Specifically, acting within the subspace $V_{(r+1)}$, we have:

$$L_{r+1}U_{r+1} = F_{r+1} \quad (4)$$

Focusing on two-dimensional space (i.e., f(x, y)∈$L_2(R^2)$), there exists one scaling function (ϕ(x,y)) and three wavelet functions ($\Psi^{(I)}$, $\Psi^{(II)}$, $\Psi^{(III)}$), defined such that:

$$\phi(x,y)=\varphi(x)\varphi(y), \Psi^{(I)}(x,y)=\varphi(X)\psi(y), \Psi^{(II)}(x,y)=\psi(X)\varphi(y), \text{ and } \Psi^{(III)}(x,y)=\psi(X)\psi(Y)$$

Expanding these functions in terms of their dilation (j) and translation parameters (k, l) we have:

$$\begin{aligned}\phi_{k,l}^{j}(x,y) &= 2^j\phi(2^j x-k,\ 2^j y-l)\\ \psi_{k,l}^{(I)j}(x,y) &= 2^j\psi^{(I)}(2^j x-k,\ 2^j y-l)\\ \psi_{k,l}^{(II)j}(x,y) &= 2^j\psi^{(II)}(2^j x-k,\ 2^j y-l)\\ \psi_{k,l}^{(III)j}(x,y) &= 2^j\psi^{(III)}(2^j x-k,\ 2^j y-l)\end{aligned} \quad (5)$$

As in the 1D case, we can write the scaling functions in terms of a set of nested subspaces (V_j).

$$v_j = span\{\Phi_{j,k_1}\otimes\Phi_{j,k_2}, k_i\in Z\} \quad (6)$$

The wavelet functions, while not forming a nested subspace, are nevertheless orthogonal and span the space given by:

$$w_j = span\{\psi_{j,k_3}\otimes\Phi_{j,k_4}, \Phi_{j,k_5}\otimes\psi_{j,k_6}, \psi_{j,k_7}\otimes\psi_{j,k_8} k_i\in Z\} \quad (7)$$

In practical terms, the wavelet transform function may be expressed in terms of its projection operators ($PQ_1Q_2Q_3$):

$$w_j = \begin{pmatrix}P\\ Q_1\\ Q_2\\ Q_3\end{pmatrix}, \begin{aligned}&P: V_j\otimes V_j\to V_{j-1}\otimes V_{j-1}\\ &Q_1: V_j\otimes V_j\to V_{j-1}\otimes W_{j-1}\\ &Q_2: V_j\otimes V_j\to W_{j-1}\otimes V_{j-1}\\ &Q_3: V_j\otimes V_j\to W_{j-1}\otimes W_{j-1}\end{aligned} \quad (8)$$

Where $P=P_xP_y$, $Q_1=P_xQ_y$, $Q_2=Q_xP_y$ and $Q_3=Q_xQ_y$.

Using the Haar [31] basis, the discrete form of operators P_r and Q_r may be expressed as:

$$P_r = \frac{1}{\sqrt{2}}\begin{bmatrix}1&1&0&0&\cdots&0&0\\ 0&0&1&1&\cdots&0&0\\ \vdots&\vdots&\vdots&\vdots&\cdots&\vdots&\vdots\\ 0&0&0&0&\cdots&1&1\end{bmatrix}_{2^{r-1}\times 2^r} \quad (9)$$

$$Q_r = \frac{1}{\sqrt{2}}\begin{bmatrix}1&-1&0&0&\cdots&0&0\\ 0&0&1&-1&\cdots&0&0\\ \vdots&\vdots&\vdots&\vdots&\cdots&\vdots&\vdots\\ 0&0&0&0&\cdots&1&-1\end{bmatrix}_{2^{r-1}\times 2^r} \quad (10)$$

Applying the transformation W_j to Eq. 17 we may write:

$$WLW^TWU = WF \quad (11)$$

Or in terms of the scaling and wavelet transform operators

$$\begin{pmatrix}P\\ Q_1\\ Q_2\\ Q_3\end{pmatrix} L\left(P^TQ_1^TQ_2^TQ_3^T\right)\begin{pmatrix}U^c\\ U_1^d\\ U_2^d\\ U_3^d\end{pmatrix} = \begin{pmatrix}F^c\\ F_1^d\\ F_2^d\\ F_3^d\end{pmatrix} \quad (12)$$

where: $U^c = PU, U_1^d = Q_1U, F^c = PF$, etc.

Letting:

$$M_{11}=\begin{pmatrix}Q_1LQ_1^T & Q_1LQ_2^T & Q_1LQ_3^T\\ Q_2LQ_1^T & Q_2LQ_2^T & Q_2LQ_3^T\\ Q_3LQ_1^T & Q_3LQ_2^T & Q_3LQ_3^T\end{pmatrix}, M_{12}=\begin{pmatrix}Q_1LP^T\\ Q_2LP^T\\ Q_3LP^T\end{pmatrix}, U_1=\begin{pmatrix}U_1^d\\ U_2^d\\ U_3^d\end{pmatrix}, F_1=\begin{pmatrix}F_1^d\\ F_2^d\\ F_3^d\end{pmatrix} \quad (13)$$

With;

$U_2 = U^c, F_2 = F^c, and\ M_{21} = M_{12}^T$, we can write the system as:

$$\begin{pmatrix}M_{11} & M_{12}\\ M_{21} & M_{22}\end{pmatrix}\begin{pmatrix}U_1\\ U_2\end{pmatrix} = \begin{pmatrix}F_1\\ F_2\end{pmatrix} \quad (14)$$

Thus, in the case of solving for U_2:

$$U_2 = \left(M_{22} - M_{21}M_{11}^{-1}M_{12}\right) = F_2 - M_{21}M_{11}^{-1}F_1 \quad (15)$$

Analogous to the 1D case, the Schur complement [33] is defined as: $S = M_{22} - M_{21}M_{11}^{-1}M_{12}$. And setting $g = F_2 - M_{21}M_{11}^{-1}F_1$, we see that $U_2 = gS^{-1}$

In this work, the aforementioned wavelet-based MRA process will be applied to several different linear PDE's belonging to each of the three primary PDE classifications, namely; parabolic, elliptical, and hyperbolic. As shown in Table 1, these classifications are distinguished by the sign of the discriminant (i.e., d^2-4ac), and prescribed in accordance with the generalized 2nd order, linear PDE. Also shown in Table 1 are some typical example applications within each subclass that are often encountered.

Table 1: PDE subclasses, worked equations and example applications.

General 2nd Order, Linear Equation		
$a(x,y)\frac{\partial^2U}{\partial x^2}+b(x,y)\frac{\partial^2U}{\partial x\partial y}+c(x,y)\frac{\partial^2U}{\partial y^2}+d(x,y)\frac{\partial u}{\partial x}+e(x,y)\frac{\partial u}{\partial y}+f(x,y)u=g(x,y)$		
Subclass	Equations	Example Applications
Parabolic (d^2-4ac=0)	(37-39)	Time dependent phenomenon: heat conduction, particle diffusion, derivative investments (Black-Scholes)
Elliptical (d^2-4ac<0)	(40-41)	Steady-State phenomenon: heat transfer, EM, fluid mechanics, etc. (Laplace, Poisson, Helmholtz.)
Hyperbolic (d^2-4ac>0)	(42-43)	Wave phenomenon: Acoustics, elastic, EM, gravitational

Result

Parabolic

The wavelet-based MRA method (described in Section 2) was first developed for use with several parabolic PDE's; namely general, second order, linear (two point) boundary value problems in one dimension. In particular, three candidate PDE's (specified below as Equations 37-39) were solved using the wavelet-based

MRA approach at various scale levels. "Exact" solutions using the finite difference method are also shown for comparison purposes. The details follow, including various notes related to the solution process for each case.

$$\frac{d^2y(x)}{dx}+1=0;\ \text{for}\ x=[0,1]\in R;\ y(0)=y(1)=0 \quad (16)$$

$$\frac{d^2x(t)}{dt}+x=5\cos(4t);\ \text{for}\ t=[0,6]\in R;\ x(0)=1,\ x(6)=0.5 \quad (17)$$

$$\frac{d^2\phi(r)}{dr}=-r\exp(-r)/2;\ for\ r=[0,\infty)\in R;\ \phi(0)=0,\ \phi(\infty)=1 \quad (18)$$

The exact solution for each of the above equations was solved using the second order finite difference method with Gaussian elimination and a mesh resolution of 2^{10} nodes. Scaled wavelet-based MRA solutions were conducted over a maximum of six scales using the Haar [31] wavelet and scaling functions (see Figure 1(a)). As indicated in Figure 2, for each of the PDE's, higher scale levels corresponded to closer agreement with the finite difference ("Exact") solutions, while significant disparities with the exact solutions were observed at lower scales. In the latter case for example, since all the wavelet-based MRA scaled solutions involved dyadic scaling (i.e., 2^j, with j = scale level), for j = 1 there exists (for each case) only one intermediate point value between the known boundary conditions. Finally, it should be noted that while the use of the Schur complement [33] obviates the need to have an a-priori exact solution, the possession of the latter does allow for scaled solutions using, for example the Haar [31] projection operations shown in Equation 9&10.

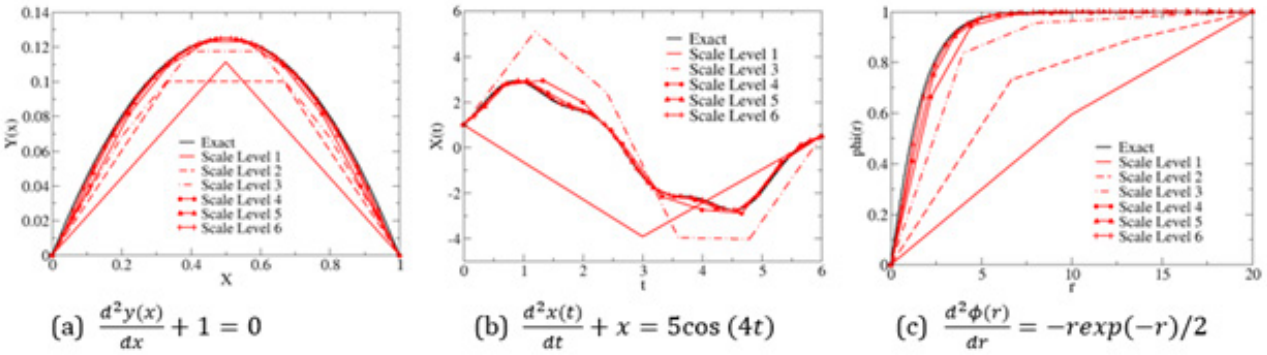

Figure 2: Exact and scaled solutions of selected one-dimensional, parabolic PDE's.

Elliptical

Next, two different elliptical PDE's were solved using the two-dimensional wavelet-based MRA method outlined in Section 2. As in the parabolic case, the multiscale solutions were carried out over six scale levels while comparisons with the exact solution were conducted using the finite difference method.

$$\frac{\partial^2U}{\partial x^2}+\frac{\partial^2U}{\partial y^2}=0\ \ for\ \ x,y=[0,1]\times[0,1]\in R^2;$$
$$U(0,y)=U(1,y)=2.0,\ U(x,0)=U(x,1)=4.0 \quad (19)$$

$$\frac{\partial^2U(x,y)}{\partial x^2}+\frac{\partial^2U(x,y)}{\partial y^2}+U(x,y)=0\ for\ x,y=[-3,3]\times[-3,3]\in R^2;$$
$$U(x,y)=\sin\left(\frac{\pi x}{6}\right)\ on\ \partial R \quad (20)$$

The two-dimensional wavelet-based MRA method was formulated in accordance with the method outlined in Section 2. The Haar [31] wavelet and scaling functions were used to solve Equation 19 & 20 from j=2 to j=6 scale levels (Figures 3&4) and normalization was conducted (based on maximum values) for purposes of comparison, and applied to both the exact and wavelet-based MRA results. The exact solution was solved via finite differences with a mesh resolution of $(2^6)^2$ grid points.

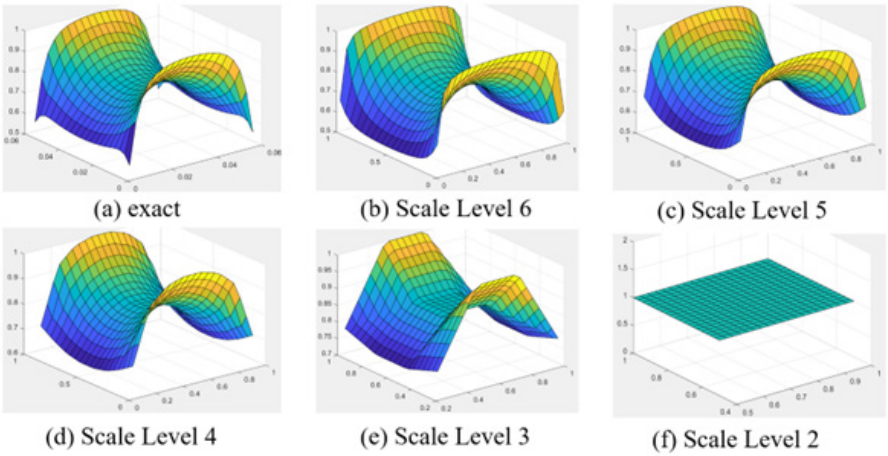

Figure 3: Comparison of exact and wavelet-based MRA scaled solutions of (∂^2 U)/(∂x^2)+(∂^2 U)/(∂y^2)=0. .

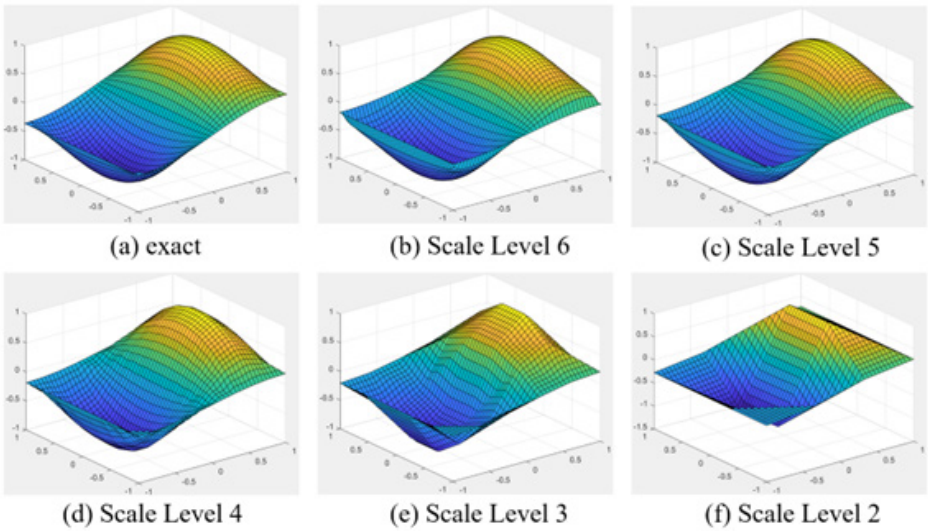

Figure 4: Exact and wavelet-based MRA scale solutions of (∂^2 U(x,y))/(∂x^2)+(∂^2 U(x,y))/(∂y^2)+U(x,y)=0. .

Hyperbolic

Finally, we investigate the wavelet-based MRA method to solve one and two dimensional hyperbolic PDE's, utilizing the aforementioned approaches contained in Section 2. Specific to the two-dimensional case, the Crank-Nicholson (implicit) solution method was utilized for achieving expressions for the tridiagonal, block coefficient matrix (L and the constant matrix F (i.e. LU=F). Again, the wavelet-based MRA method was formulated with Haar [31] wavelet and scaling functions and were used to solve each equation from j=4 to j=8 scale levels. The exact solution was solved via finite differences with a mesh resolution of 2^8 grid points.

$$\frac{\partial U(x,t)}{\partial t}+V\frac{\partial U(x,t)}{\partial t}=0 \ \ for \ x=[0,100]\in R, t\geq 0;$$
$$U(x,0)=\exp(-0.01(x-45)^2); 20\leq x\leq 70 \quad (21)$$

$$\frac{\partial^2 U}{\partial t^2}=c^2\left(\frac{\partial^2 U}{\partial x^2}+\frac{\partial^2 U}{\partial y^2}\right) \ \ for \ x,y=[0,1]\times[0,1]\in R^2, \ t\geq 0, \ c=2;$$
$$u(x,y,0)=\sin(\pi x)\sin(2\pi y); \ \ u(0,y,t)=u(1,y,t)=u(x,0,t)=u(x,1,t)=0 \quad (22)$$

With respect to solutions of the first hyperbolic PDE (i.e., Eq. 42), we first show only the finite difference results corresponding to the evolution of U(x) at three different velocities (V=2m/s, 4m/s and 8m/s) and at three distinct time intervals (t=0 s, 1s, 2s and 3 s.). As indicated in Figure 5, we note the anticipated linear advection of U(x) as it evolves along the x-axis and further note (as expected) that this advection increases proportionately for larger values of the constant V. Finally, as in each of the previous 'exact' cases, we observe nearly continuous function profiles for U. In Figure 6 we show results corresponding to both the finite difference and wavelet-based MRA results at time t=3 s for scale levels 4, 6 and 8. In particular, we note the relatively coarse result corresponding to scale level 4 and the expected, proximate agreement with the 'exact' solution at larger scales. We also note that for larger values of the Velocity (V), there tends to be a lag between the exact and wavelet-based MRA results (i.e., the max value of the wavelet-based MRA results at each scale level occurs earlier than does the max value of the exact results). Figure 7 shows the finite difference and wavelet-based MRA results at times t=0 s, 1s, 2s and 3s and at a scale level of 6. Again, while the agreement between the exact solution and the wavelet-based MRA is fairly good for low values of velocity (i.e., V=2m/s), there is an observed lag with the wavelet-based MRA results that increases with V and at all times t. Finally, the two-dimensional, hyperbolic PDE (Eq. 43) is solved. In Figure 8, we show exact and wavelet-based MRA results corresponding to time t=2s, 5s and 10s. As anticipated, we note the evolution of the 2D wave with time, and observe the relatively course approximation corresponding to scale level 3 ('S3').

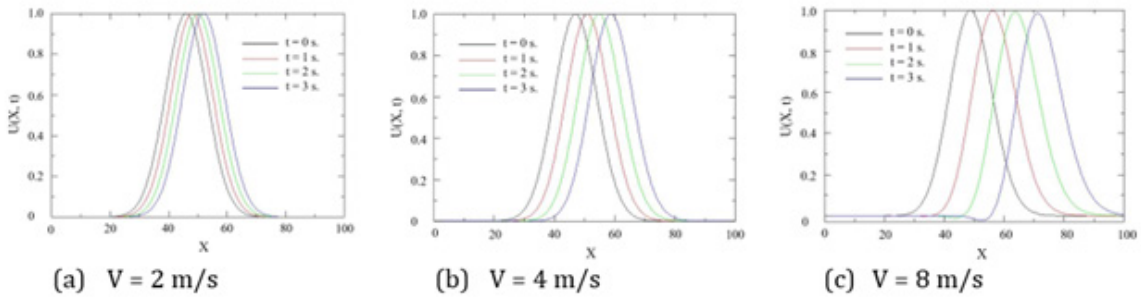

Figure 5: Exact (finite difference) solutions of (∂U(x,t))/∂t+V (∂U(x,t))/∂t=0 for variable values of V, and over discrete times t=0s, 1s, 2s., and 3s.

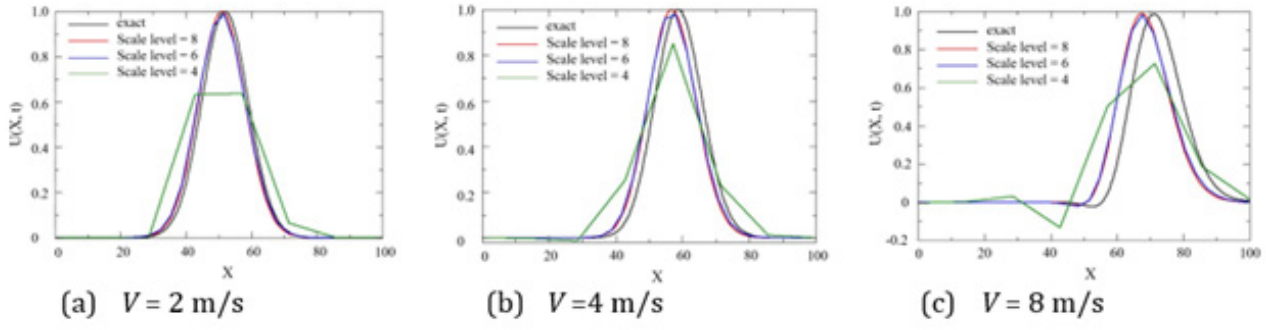

Figure 6: Comparisons of exact and wavelet-based MRA solutions of $(\partial U(x,t))/\partial t+V\ (\partial U(x,t))/\partial x=0$ for variable V, at time t=3s. and scale levels from j=4 to j=8.

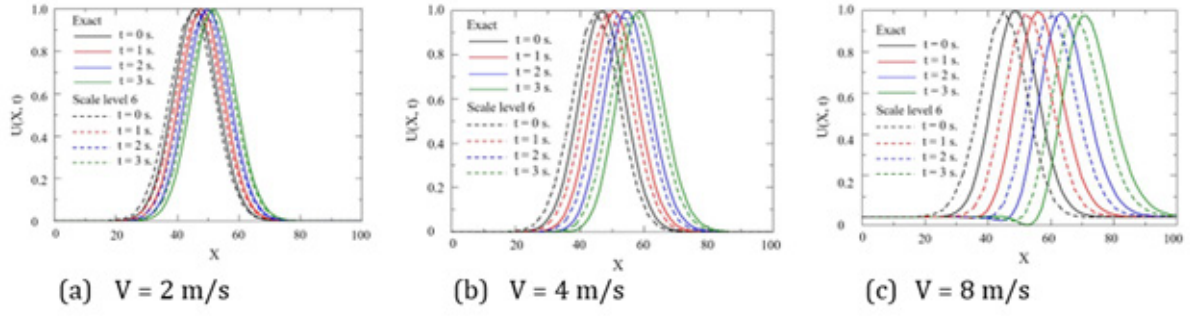

Figure 7: Comparisons of exact and wavelet-based MRA solutions of $(\partial U(x,t))/\partial t+V\ (\partial U(x,t))/\partial x=0$ for variable V, at time t=0 s. to 3s. and for scale level j=6.

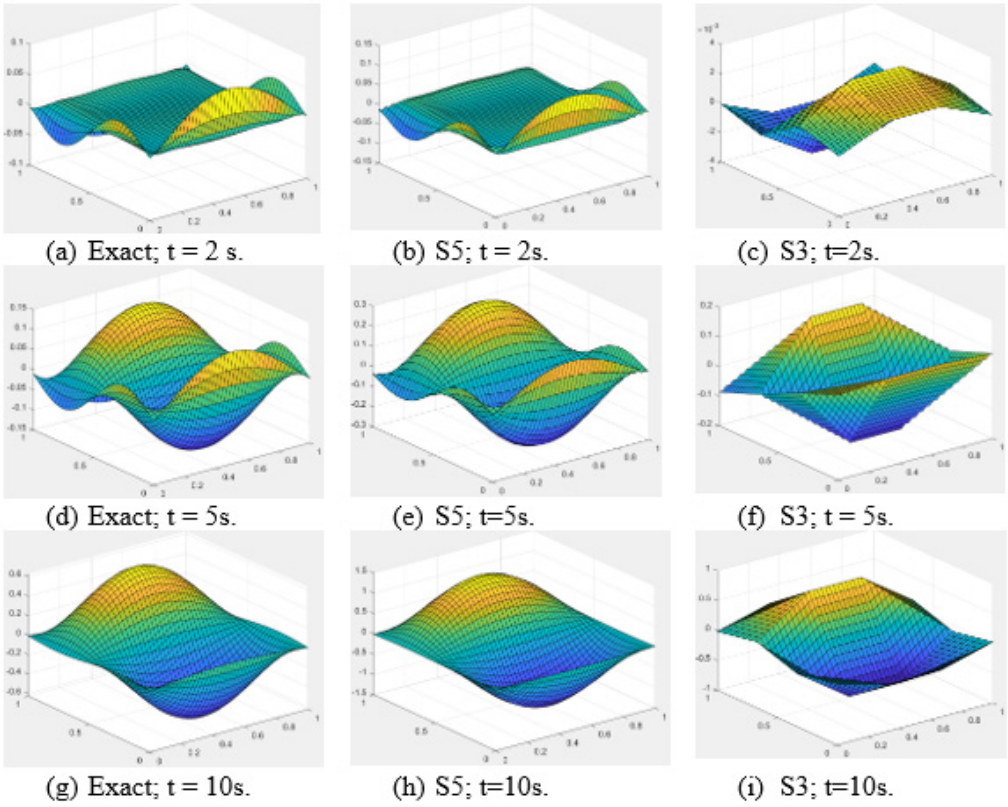

Figure 8: Exact and wavelet-based MRA scaled solutions of $(\partial^2 U)/(\partial t^2)=c^2\ ((\partial^2 U)/(\partial x^2)+(\partial^2 U)/(\partial y^2))$.

Conclusion

In this work we investigated the use of wavelet-based MRA for scaled solutions of various linear partial differential equations. In particular, we investigated exact and scaled solutions of various parabolic, elliptic, and hyperbolic PDES's in one and two dimensions. For the exact solutions, we utilized a standard Finite Difference approach with Gaussian elimination, while for the scaled solutions, we applied the wavelet-based MRA method (incorporating the Haar [31] wavelet basis and the Schur complement [33]). The findings from this work provide for the following observations:

A. The wavelet-based MRA method proved effective at offering scaled solutions for solving linear, one-dimensional, and two-dimensional, parabolic, elliptical, and hyperbolic PDE's of type: LU=F.

B. The use of the Schur complement [33] obviates the need to have an a priori exact solution, while the possession of the latter offers the use of simple projection operations.

C. For hyperbolic cases, with relatively large velocity magnitudes, an observed lag is found with respect to the wavelet-based MRA solutions when compared to the exact solutions.

Potential future efforts aligned with this study will focus on the utilization of the wavelet-based MRA method for non-linear PDE's, and the evaluation of some of the other discrete scaling and wavelet basis functions.

References

1. H Wang, M Tom, F Ou, G Orkoulas, PD Christofides (2004) Multiscale computational fluid dynamics modeling of an area-selective atomic layer deposition process using discrete feed method. Digital Chemical Engineering 10: 100140.
2. S Chen, M Wang, Z Xia (2014) Multiscale fluid mechanics and modeling. Procedia IUTAM 10: 100-114.
3. P Koumoutsakos (2005) Multiscale flow simulations using particles. Annu Rev Fluid Mech 37: 457-487.
4. Q Ren, Y Su, TA Feldhausen, RA Kurfess, KB Fillingim, et al. (2024) Multiscale characterization of an additively manufactured property graded Ni-base alloy for molten-salts/supercritical-CO_2 heat exchangers. Materials and Design 237: 112560.
5. E Giessen, PA Schultz, N Bertin, VV Bulatov, W Cai, et al. (2020) Roadmap on multiscale materials modeling. Modeling Simul Mater Sci Eng 28: 61.
6. T Su, S Huang, JG Jean, C Chen (2022) Multiscale computational solid mechanics: Data and machine learning. Journal of Mechanics 38: 568–585.
7. LR Frank, VL Galinsky, Z Zhang, FM Ralph (2024) Characterizing the dynamics of multi-scale global high impact weather events. Scientific Reports 14: 724.
8. S Ahsin, A Wajid, A Majid, H Nazneed, S Shim, et al. (2009) A hybrid model for forecasting of particulate matter concentrations based on multiscale characterization and machine learning techniques. Mathematical Biosciences & Engineering 18(3): 1992-2009.
9. JB Allen (2021) Mesoscale modeling of metal-based selective laser melting: Evolution of the vapor capillary. Materials Research Express 3(1): 015026.
10. Allen JB, GA Riveros, IP Beckman, EL Freeman (2023) Mesoscale fused deposition modeling: Extrusion and solidification. Recent Progress in Materials: Research and Development of Subtractive and Additive Manufacturing Technologies 5(4): 33.
11. P Wesseling (1992) An introduction to multigrid methods. Wiley, New Jersey, USA.
12. A Brandt (1977) Multi-level adaptive solutions to boundary value problems. Math Comp 31(138): 333-390.
13. A Toselli, O Widlund (2004) Domain decomposition methods: Algorithms and theory. Springer Series in Computational Mathematics, Springer, New York, USA.
14. S Thirunavukkarasu, M Guddati (2012) A domain decomposition method for concurrent coupling of multiscale models. Int J Numerical Methods in Engineering 92(11): 918-939.
15. M Ryvkin (2008) Employing the discrete Fourier transform in the analysis of multiscale problems. Int J Multiscale Computational Engineering 6(5): 435-449.
16. L Greengard, V Rokhlin (1987) A fast algorithm for particle simulations. J Comput Phys 73(2): 325-348.
17. DF Martin, P Colella, M Anghel, FJ Alexander (2005) Adaptive mesh refinement for multiscale nonequilibrium physics. Computing in Science and Engineering 7(3): 24-31.
18. I Daubechies (1992) Ten lectures on wavelets. SIAM Publishers, Philadelphia, USA.
19. M Brewster, G Beylkin (1995) A multiresolution strategy for numerical homogenization. Appl Comput Harmon Anal 2(4): 327-349.
20. A Bensoussan, JL Lions, GC Papanicolaou (1978) Asymptotic analysis for periodic structures. North-Holland Pub Co, Amsterdam, Netherlands.
21. GA Pavliotis, AM Stuart (2008) Multiscale methods: Averaging and homogenization, Springer-Verlag, New York, USA.
22. A Chertock, D Levy (2004) On wavelet-based numerical homogenization. Multiscale Model Simul 3(1).
23. NA Coult (1997) A multiresolution strategy for homogenization of partial differential equations. PhD Dissertation, University of Colorado, USA.
24. EB Tadmor, M Ortiz, R Phillips (1996) Quasicontinuum analysis of defects in solids. Philos Mag A 73(6): 1529-1563.
25. J Knap, M Ortiz (2001) An analysis of the quasicontinuum method. J Mech Phys Solids 49(9): 1899-1923.
26. S Mallat (1989) Multiresolution approximations and wavelet orthonormal bases of L^2. Transactions of the American Mathematical Society 315(1): 69-87.
27. C Basdevant, V Perrier, T Philipovitch (1993) Local spectral analysis of turbulent flows using wavelet transforms. In: JT Beale (Ed.), Vortex Flows and Related Numerical Methods, Kluwer Academic Publishers, Netherlands, pp. 1-26.
28. S Mehraeen, JS Chen (2004) Wavelet-based multi-scale projection method in homogenization of heterogeneous media. Finite Elements in Analysis and Design 40(12): 1665-1679.
29. JB Allen (2017) Wavelet-based numerical homogenization for scaled solutions of linear matrix equations. International Journal of Discrete Mathematics 2(1): 10-16.
30. MT Taner (1983) Joint time/frequency analysis, Q quality factor and dispersion computation using Gabor-Morlet wavelets or Gabor-Morlet transform.
31. A Haar (1910) On the theory of orthogonal function systems. Mathematical Annals 69(3): 76.
32. SP Kopysov, YA Sagdeeva (2010) Two-dimensional numerical wavelet homogenization for obtaining effective characteristics of composite materials. Mathematical Models and Computer Simulations 2(1): 103-115.
33. Z Fuzhen (2005) The Schur complement and its applications. Springer, New York, USA.